NANO LETTERS

pubs.acs.org/NanoLett

Optical Properties of Crystalline–Amorphous Core–Shell Silicon Nanowires

M. M. Adachi,*,† M. P. Anantram,‡ and K. S. Karim†

†Department of Electrical and Computer Engineering, University of Waterloo, Waterloo, Ontario N2L 3G1, Canada, and ‡Department of Electrical Engineering, University of Washington, Seattle, Washington 98195

ABSTRACT The optical absorption in a nanowire heterostructure consisting of a crystalline silicon core surrounded by a conformal shell of amorphous silicon is studied. We show that they exhibit extremely high absorption of 95% at short wavelengths (λ < 550 nm) and a concomitant very low absorption of down to less than 2% at long wavelengths (λ > 780 nm). These results indicate that our nanowires do not have optically active energy levels in the band gap. The absorption edge of silicon nanowires arrays is observed to shift to longer wavelengths as a function of the overall nanowire diameter. The near-infrared absorption of the nanowire array is significantly better than that of thin film amorphous silicon. These properties indicate potential use in large area optoelectronic and photovoltaic applications.

KEYWORDS Silicon nanowires, heterostructure, optical properties, absorption, reflectance

Silicon nanowires have attracted much interest due to potential advantageous optical,[1,2] thermoelectric,[3] and electronic properties.[4] Growth of crystalline-silicon-core–amorphous-silicon-shell heterostructure nanowires have also been reported previously[5] and have been used in applications including battery electrodes[6] and electrical switches.[7] However the optical properties of heterostructure nanowires have not been investigated to the best of our knowledge. Crystalline silicon nanowire samples have been shown to enhance optical absorption[2,8,9] in the visible and near-infrared regions when compared to thin film crystalline silicon. The band gap of low dimensional crystalline silicon nanowires can also be engineered by controlling the nanowire diameter (1–7 nm)[10] or introducing strain.[11] Amorphous silicon nanowires and nanocones have also been fabricated using a top-down etching approach and have been shown to exhibit much higher absorption between wavelengths of 400 and 800 nm compared to thin film amorphous silicon.[12] Heterostructure nanowires offer a number of advantages over purely crystalline silicon nanowires. First, amorphous silicon is capable of simultaneously providing excellent surface passivation for crystalline silicon and creating a p–n junction in high efficiency heterojunctions a-Si/crystalline silicon solar cells.[13] Passivation of surface defects is necessary for attaining high electronic mobilities in nanowire devices.[4] Second, the high absorption coefficient of amorphous silicon facilitates very high absorption even for short nanowire arrays having lengths of about 1.28 μm, shown in this study. The advantage of the heterostructure nanowires used in this study as compared to purely amorphous silicon nanowires is that the crystalline core can be used as an efficient electrical conducting pathway[6] which is particularly useful considering the low mobility ($\tau_e \sim 10$ cm^2/(V s)) of amorphous silicon due the disorder in atomic structure.[33] The optical properties of crystalline–amorphous silicon heterostructure nanowires are investigated for large area device applications.

Silicon nanowires have also been grown using a number of different techniques such as evaporation,[15] solution-based methods,[16] and top-down etching.[12,17] The most common bottom up growth method is the metal catalyzed vapor–liquid–solid (VLS) method.[18–20] The approach adopted in this paper is the plasma-enhanced chemical vapor deposition (PECVD) approach.[21] The role of the plasma is to preionize the source gas and provide local surface heating significantly increasing higher nanowire growth rates at low substrate temperatures.[21] Furthermore, the plasma was found necessary in this work for nanowire growth when using a Sn catalyst at the low growth temperature of 400 °C.

Catalyst nanoislands based on a variety of elements, such as Pt, Ag, Pd, Cu, Ni,[18] Al,[22] Fe,[15] Ga,[23] In,[24] Zn,[25] Co,[26] Ti,[27] and Sn,[28–30] have been used to grow silicon nanowires. Au, Fe, and Ti dissolved in silicon create deep trap states in the band gap and significantly degrade crystalline silicon solar cell performance.[31] For large area thin film applications, desirable characteristics of the catalyst include low eutectic temperature with Si, low solubility in Si, and high threshold concentration before device performance degradation. Catalysts that have a low eutectic point with silicon and also have low solubility in silicon include Bi, In, Sn, and Ga. Sn has a very high threshold concentration before performance degrades in crystalline silicon solar cells.[31] Further Sn has a eutectic temperature of 231.9 °C. In addition, Trumbore et al. investigated the electrical properties of crystalline silicon with grown-in Sn and found Sn was not an effective recombination center for holes and electrons.[32]

* To whom correspondence should be addressed, mmadachi@uwaterloo.ca.
Received for review: 06/21/2010
Published on Web: 09/03/2010

© 2010 American Chemical Society

DOI: 10.1021/nl102183x | *Nano Lett.* **2010,** *10,* 4093–4098

Using the transfer matrix method, Hu et al. calculated that crystalline silicon nanowires have enhanced absorption at short wavelengths but poorer absorption at long wavelengths as compared to bulk crystalline silicon[1] but there has been no clear experimental proof of this. Crystalline silicon does not efficiently absorb light at near band gap energies because it is an indirect band gap semiconductor. At near band gap energies, optical absorption/emission is a weak process in indirect band gap materials because both a phonon (for momentum conservation) and photon (for energy conservation) need to simultaneously participate. In contrast, amorphous silicon (a-Si) absorbs photons more efficiently because a phonon is not required due to the lack of long-range order[33] and it is well-known that very thin films of amorphous silicon efficiently absorb light.

In this study, the optical properties of a heterostructure consisting of a crystalline silicon core and a conformal amorphous silicon shell is investigated for the first time. The nanowires are heterostructures in the radial direction, where the band gap of the core is smaller than the band gap of the shell. Our central results are that the optical absorption is extremely high (95%) at short wavelengths ($\lambda < 550$ nm) and falls to very low values (<2%) at long wavelengths ($\lambda > 780$ nm) for an array consisting of our smallest diameter nanowires (15−40 nm). As the nanowire diameter increases, the absorption edge shifts to longer wavelengths. It is important to note that we have demonstrated that our nanowire array shows (i) efficient absorption over longer wavelengths where thin film a-Si is transparent and (ii) superior absorption at short wavelengths compared to both bulk crystalline and amorphous silicon. The silicon nanowires are grown by PECVD using a Sn catalyst at a substrate temperature of 400 °C so that low-cost substrates such as glass can be used for large area applications.

Experiment. Silicon nanowires were grown by the vapor−liquid−solid (VLS) method in a commercial MVSystems, Inc., rf parallel plate PECVD system. Nanowires were grown on two substrates: p-type (100) Si wafers and Corning 1737 glass. The native oxide on the Si substrate was not removed, and as a result nanowires grew in a window of angles around the normal to the substrate. The wafers were cleaned by RCA1 solution, and the glass substrates were cleaned in an acetone immersed ultrasonic bath followed by an isopropyl alcohol immersed ultrasonic bath.

Thin films of Sn with a thickness of 2 nm were deposited by e-beam evaporation at a base pressure $<1 \times 10^{-6}$ Torr. The thickness of the Sn film was determined using a well-calibrated quartz crystal thickness monitor. Samples were transferred to the PECVD chamber and preheated using a heater well that is located behind the substrate for approximately 1 h at a base pressure of $\sim 1 \times 10^{-6}$ Torr. During this step the catalyst film agglomerated to form nanoislands. Silane was used as the Si source gas, and the plasma was created by a conventional 13.56 MHz rf supply with an electrode spacing of 2 cm. The power density supplied by the rf source was controlled from 0.0137 to 0.0215 W/cm^2, for 30 min for each sample grown. The preheat and deposition substrate temperatures were both 400 °C. Deposition pressure was controlled using an automatically adjusted throttle valve and was set to 1400 mTorr. The silane flow rate was 20 sccm (standard cubic centimeters per minute), which was controlled using a mass flow controller. The conditions specified above applied uniformly to all samples grown on both the silicon and glass substrates.

The diameter and length distribution of silicon nanowires were characterized by scanning electron microscopy (SEM) for samples grown on silicon substrate. Nanowire diameters were measured from planar SEM micrographs, and their length was calculated by taking the average length of the 10 longest nanowires in cross-sectional SEM micrographs. SEM measurements of silicon nanowires were taken on both glass substrate and Si substrates, and diameters were found to agree within 10%. Si substrates were used for the reported SEM images since thermal drift was observed to lower the quality of measurements of samples on glass substrates. The thickness of the uncatalyzed a-Si on the substrate was measured from cross-sectional SEM micrographs. A LEO 1530 field-emission SEM was used for all measurements.

Nanowires that were grown in the same PECVD chamber under identical growth conditions on the glass substrate were characterized by the following methods: UV−vis−NIR spectroscopy, X-ray diffraction, Raman spectroscopy, transmission electron microscopy (TEM), and energy dispersive X-ray fluorescence (EDX) measurements. The crystalline structure of nanowires was characterized using X-ray diffraction (PANalytical X'Pert PRO X-ray diffractometer) and a Renishaw Raman spectrometer in a backscattering setup with 633 nm laser excitation. The total optical transmission and reflectance (including both specular and diffuse components) were measured using a Varian Cary 5000 UV−vis−NIR spectrophotometer equipped with an integrating sphere. A baseline correction was performed with no sample before performing total transmission measurements. The total reflectance measurements were calibrated using Labsphere, Inc., Spectralon Diffuse Reflectance Standards prior to measurements. TEM micrographs were measured using a JEOL 2010 field emission TEM equipped with an energy dispersive X-ray spectrometer (EDS). TEM samples were prepared by scraping a holey-carbon TEM grid over a nanowire-covered glass sample.

Results and Discussion. ***Structural Analysis.*** Figure 1a shows a planar-view SEM micrograph of Sn catalyst islands with diameters ranging between 5 and 10 nm which was formed after annealing the 2 nm thick Sn film. The diameters of the silicon nanowires grown on the silicon substrate using the catalyst shown in Figure 1a at a power density of 0.0164 W/cm^2 range from 30 to 60 nm as shown in the cross-sectional SEM micrograph in Figure 1b.

The high-resolution TEM micrograph of a silicon nanowire grown at the same deposition conditions as in Figure 1b is

© 2010 American Chemical Society

DOI: 10.1021/nl102183x | *Nano Lett.* **2010,** *10,* 4093–4098

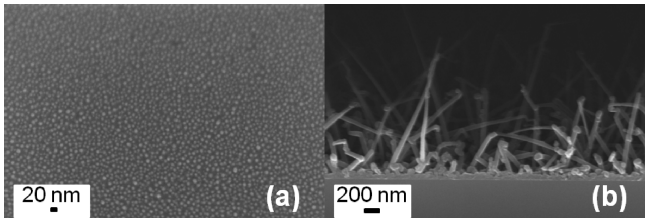


FIGURE 1. SEM micrograph of (a) planar view of Sn catalyst islands after annealing a 2 nm thick Sn film and (b) cross-sectional view of silicon nanowires grown by PECVD with diameters of 30−60 nm.

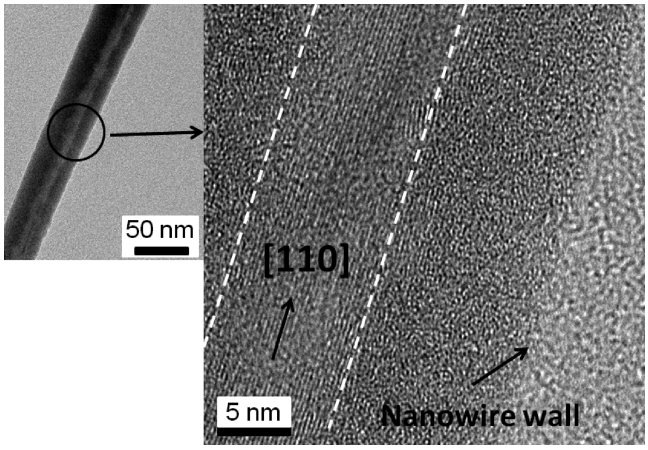


FIGURE 2. High-resolution TEM micrograph of a silicon nanowire grown at a power density of $P = 0.0164$ W/cm^2 deposition pressure of 1400 mTorr growth time of 30 min. The nanowire consists of a highly crystalline core with visible Si(111) lattice fringes with a lattice spacing of 0.31 nm surrounded by an amorphous shell. The nanowire growth direction is [110]. The lighter amorphous pattern in the background located to the right of the nanowire wall is the carbon TEM grid.

shown in Figure 2. The nanowire consists of a highly crystalline core with visible Si(111) lattice fringes separated by a spacing of 0.31 nm. The crystalline core has a diameter of 9.2 nm and has a growth direction of [110] surrounded by an amorphous shell resulting in a total nanowire diameter of around 42 nm. Note that the crystalline core is not centered within the surrounding amorphous shell because deposition favored one side over the other due to slanting of the nanowire during growth.

Energy dispersive X-ray fluorescence (EDX) on the nanowire sample showed a huge Si peak followed by a tiny O peak, which may have originated from a thin layer of native surface oxide. The EDX measurements did not detect the presence of Sn either through the center of the nanowire or at the nanowire tip. The latter indicates that nanowire growth ceased because the Sn catalyst was either consumed or evaporated. Note that some silicon nanowires were observed to lack a crystalline core and instead consisted of small crystallites surrounded by an amorphous silicon matrix.

The effect of plasma power on nanowire structure, crystallinity and optical properties was investigated. SEM micrographs of nanowires grown at four different power densities are shown in Figure 3, and a summary of measured nanowire lengths, diameters, and uncatalyzed a-Si thicknesses on the substrate is shown in Table 1. No nanowire growth was observed at the lowest power density of 0.0137 W/cm^2 as shown in Figure 3a. The use of plasma was found necessary for silicon nanowire growth from Sn catalyst at the relatively low growth temperature of 400 °C used in this study. Increasing the power density to 0.0156 W/cm^2 resulted in a dense array of silicon nanowires as shown in Figure 3b. An increase in the nanowire diameter and the thickness of the amorphous shell was observed with increase in power density. Table 1 also shows that an increase in deposition power density leads to a thicker uncatalyzed a-Si film on the silicon substrate located below the nanowires.

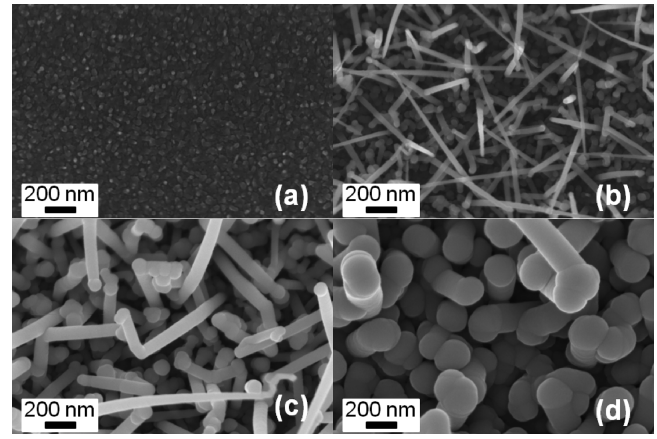


FIGURE 3. Planar SEM micrographs of nanowires grown at different power densities of (a) $P = 0.0137$ W/cm^2, (b) $P = 0.0156$ W/cm^2, (c) $P = 0.0176$ W/cm^2, and (d) $P = 0.0195$ W/cm^2.

TABLE 1. Summary of the Effect of Deposition Power Density on Silicon Nanowire (NW) Diameter, NW Length, and Uncatalyzed a-Si Thickness on the Substrate

deposition power density (W/cm^2)	total NW diameter (nm)	NW length (nm)	a-Si layer thickness on substrate (nm)
0.0137	no nanowires		
0.0156	15−40	1738	60
0.0164	30−60	2289	80
0.0176	55−90	2100	80
0.0195	150−180	1282	100

From Table 1, the longest average nanowire length measured was 2289 nm, which corresponds to a power density of $P = 0.0164$ W/cm^2. As the power was increased further, the nanowire length decreases along with an increase in the thickness of the a-Si on the nanowire. Silicon nanowires cease growing if the catalyst is consumed or the deposition conditions are changed.[18] Since the deposition conditions were kept constant, the catalyst was likely consumed. If the power density was increased to $P = 0.0195$ W/cm^2, the nanowire length decreased to 1282 nm while the uncatalyzed a-Si thickness increased to 100 nm suggesting the competing uncatalyzed a-Si deposition led to suppression of nanowire growth. In fact if the power was increased to 0.0438 W/cm^2, nanowire growth was suppressed further resulting in only large bumps.

© 2010 American Chemical Society

DOI: 10.1021/nl102183x | Nano Lett. 2010, 10, 4093–4098

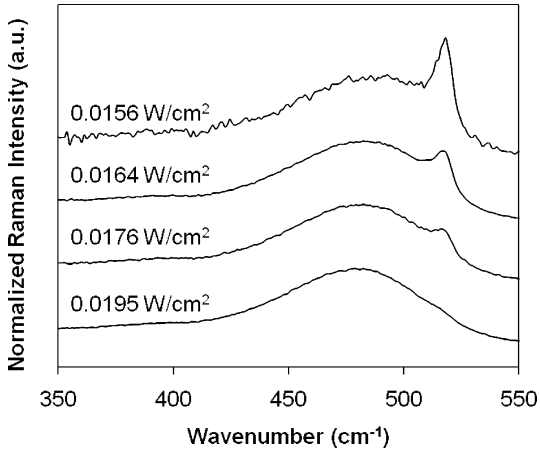


FIGURE 4. The Raman spectra of silicon nanowires grown at different power densities indicate increasing amorphous silicon coverage (broad peak at 480 cm^{-1}) with power density. The sharp peak at 520 cm^{-1} is the signature of crystalline silicon in the nanowires.

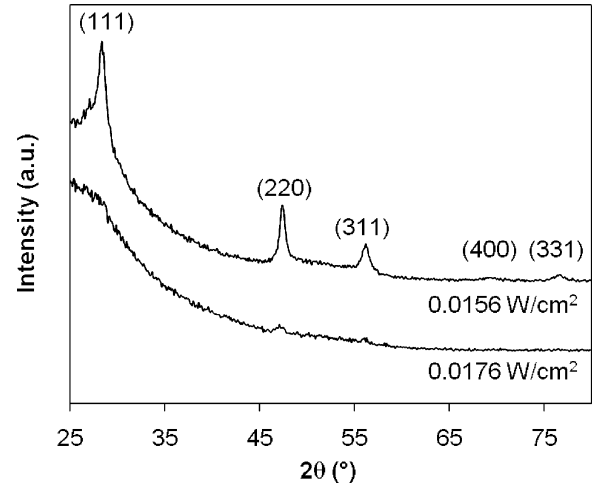


FIGURE 5. XRD intensity of silicon nanowires grown at two different power densities, 0.0156 and 0.0176 W/cm^2. The crystal orientations corresponding to XRD peaks are shown in brackets. The nanowires grown at 0.0156 W/cm^2 have highly crystalline (111), (220), and (311) peaks. The same peaks for the nanowires grown at 0.0176 W/cm^2 are suppressed by the amorphous silicon shell.

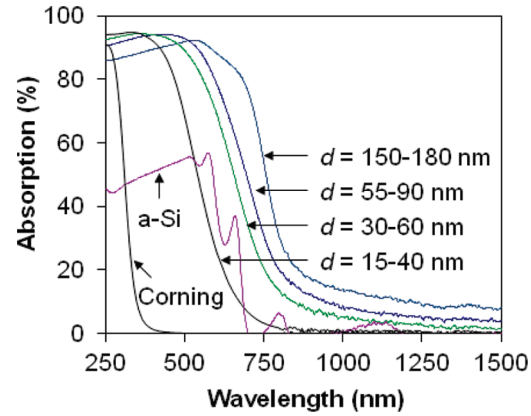


FIGURE 6. Absorption ($1 - T - R$) as a function of wavelength for silicon nanowires with varying total diameters, d. The diameter is controlled by adjusting the plasma power density which increases the amorphous silicon shell thickness. The absorption of a thin film of a-Si with a thickness of $t = 400$ nm is also shown for comparison. For the lowest diameter silicon nanowire array of $d = 15-40$ nm, the short wavelength absorption is very high (95%) but drops abruptly to <2% for longer wavelengths, $\lambda > 780$ nm. The absorption edge of silicon nanowires shifts to longer wavelengths for increasing total diameter well beyond the absorption limit of thin film amorphous silicon.

The transition from nanowire growth to conformal uncatalyzed amorphous silicon growth can be identified from the nanowire crystallinity. The normalized Raman spectra for nanowires grown at four different power densities are shown in Figure 4. The sharp peak at 520 cm^{-1} is from crystalline silicon and the broad peak at 480 cm^{-1} is due to scattering from amorphous silicon. The crystalline silicon peak decreases for increasing power density because of increased coverage of uncatalyzed amorphous silicon. Note that the broad amorphous peak is present even at the lowest power and is due to uncatalyzed a-Si located on the nanowires and on the substrate.

The crystalline structure of silicon nanowires grown for two different power densities of $P = 0.0156$ W/cm^2 and $P = 0.0176$ W/cm^2 was also characterized by X-ray diffraction. The XRD spectra are shown in Figure 5. Nanowires grown at 0.0156 W/cm^2 have large (111), (220), (311) crystalline peaks and small peaks at (400) and (331). Solving for the Scherrer formula ($dk\lambda/\beta \cos \theta$), the crystalline size was estimated to be 12.9 nm from the (111) XRD peak, which compares well to that of the crystalline core with a diameter of 9.2 nm measured by TEM (Figure 2). The XRD pattern for nanowires grown at $P = 0.0176$ W/cm^2 is shown for comparison. The coverage by amorphous silicon strongly scattered the X-rays which suppressed the peaks of the crystalline core of the nanowires.

Optical Properties. The effect of the amorphous silicon shell in influencing the optical properties was investigated by transmission and reflection measurements. Figure 6 shows the effective optical absorption of silicon nanowires with varying diameters. The absorption is defined as $1 - T - R$ where T is the total transmission and R is the total reflectance. For comparison, the absorption and total reflectance of a thin film of 400 nm thick a-Si are shown in Figure 6. The absorption by the a-Si film is limited to <55% for all wavelengths due to the large reflectance shown in Figure 7b.

At low incident optical wavelengths, all nanowires show a very high absorption of between 85 and 95%, depending on the nanowire diameter. High absorption by VLS grown silicon nanowires has been reported previously[2,8] and is attributed to enhanced light trapping (i.e., increasing the path length of incoming light) in nanowire arrays. Nanowires grown from the VLS method consist of a distribution of diameters[20,2,8] mainly due to variation in the initial catalyst nanoparticle size. As a result each absorption curve in Figure 6 is due to the overall absorption for an array of nanowires consisting of the specified range of diameters.

© 2010 American Chemical Society

DOI: 10.1021/nl102183x | *Nano Lett.* **2010,** *10,* 4093–4098

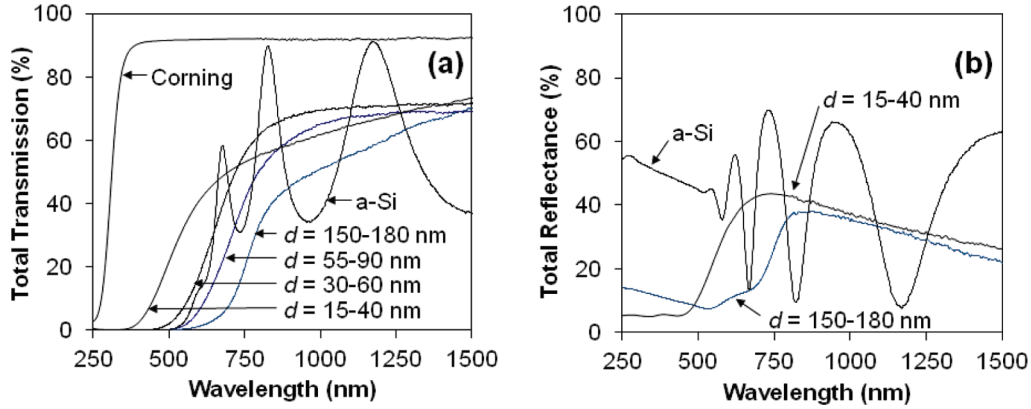


FIGURE 7. (a) Total transmission and (b) total reflectance as a function of wavelength for different total diameters, *d*. The transmission is zero at short wavelengths and becomes nonzero at wavelengths dependent on *d*.

A significant feature of absorption spectra is the rather abrupt drop in absorption for all nanowire diameters with the drop extending to longer wavelengths from $\lambda \sim 550$ to 760 nm as the diameter increases. While the shift in wavelength corresponds qualitatively to the increase in band gap with decrease in diameter, we rule this out based on the fact that the TEM images of our samples show that the crystalline core has a diameter of about 9.2 nm, where quantization effects are weak. Rather, the shift in absorption edge is better explained by increase in the filling ratio (i.e., the area ratio between nanowires and substrate). In this work, the density of nanowires (i.e., number of nanowires per area) agree within a measurement error of 10% for the first three nanowire arrays ($d = 15-40$ nm, $d = 30-60$ nm, and $d = 55-90$ nm). As a result an increase in amorphous shell thickness results in an increase in filling ratio. The same trend of absorption edge shift to longer wavelengths as a function of increase in filling ratio was calculated by Hu et al. for vertically aligned silicon nanowires.[1] A difference between our experimental samples and the model used in theoretical work[1] is that our low temperature samples grow within a window of angles around the normal to the substrate. Theoretical verification of this feature for randomly oriented nanowires would be of great use to groups involved in low-temperature growth of nanowires.

The nanowire array with the largest total diameter of $d = 150-180$ nm has a lower nanowire density than the smaller diameter arrays because neighboring nanowires merge with each other. Nevertheless, the same trend of increase in long wavelength absorption was observed for the $d = 150-180$ nm array in Figure 6. Interestingly the long wavelength absorption is highest for this diameter even though the length of these wires is considerably shorter at 1.28 μm. The band gap of a-Si is around 1.78 eV (wavelength ~700 nm). However we see absorption at significantly longer wavelengths (for example 54% absorption at 750 nm) which can be attributed to enhanced light trapping ability of nanowires. The absorption could originate from the crystalline silicon core absorbing light at the wavelengths that correspond to energies longer than that of the a-Si band gap and absorption due to bandtails of a-Si.

A second significant feature from Figure 6a is the sudden drop in absorption at wavelengths comparable to the band gap of amorphous silicon (1.78 eV). The sub-band-gap absorption ($\lambda > 1200$ nm) drops to values smaller than 10% in all samples, considerably lower than that reported by nanowires grown using Au catalyst.[2,8] In fact, using a comparable catalyst thickness of 2.5 nm as opposed to the 2 nm used in this work, the sub-band-gap absorption for Au-catalyzed silicon nanowires was reported to be up to 55% at $\lambda = 1200$ nm.[2] This suggests that the type of catalyst used during nanowire growth using the VLS method has a strong influence on sub-band-gap optical absorption. In fact, sub-band-gap optical absorption has also been reported in microstructured silicon spikes[34] and the chemical impurities (i.e., sulfur) present at the surface of the spikes were believed to be the main contributor of the sub-band-gap absorption.[34] In contrast the optical absorption of our nanowires points to the absence of optically active energy levels in the band gap, a key requirement for photovoltaic and optoelectronic applications. Such energy levels give rise to trap-assisted recombination, lowering carrier lifetimes and collection efficiencies.

Figure 7 shows the total transmission and total reflectance of silicon nanowire arrays as a function of wavelength with varying total diameters, *d*. The absorption edge shift observed in Figure 6a is due to the shift in the wavelength at which transmission increases abruptly in Figure 7a for different *d*. The total reflectance also shows the same trend. The color of nanowire arrays was observed to change from light orange to brown to dark purple with increase in nanowire diameter.

Conclusion. The optical properties of a heterostructure consisting of a crystalline silicon core and a conformal amorphous shell were investigated for the first time. For an array consisting of our smallest diameter nanowires (15−40 nm) the optical absorption is very high (95%) at short wavelengths ($\lambda < 550$ nm) and drops sharply to very low

© 2010 American Chemical Society

DOI: 10.1021/nl102183x | *Nano Lett.* **2010,** *10,* 4093–4098

values (less than 2 %) at long wavelengths ($\lambda > 780$ nm). Such silicon nanowires have potential applications in large area optical filters, selected area (defined by lithography) antiscatter material, or photodetectors with wavelength selectivity controlled by nanowire diameter. The absence of optically active energy levels in the band gap is important for applications such as photodetectors and solar cells. As the overall nanowire diameter increases, the absorption edge shifts to longer wavelengths. The largest diameter nanowires (150−180 nm) showed significantly higher long wavelength absorption (54 % at 750 nm) as compared to an a-Si film (0 % at 750 nm). Heterostructure silicon nanowires showed significantly higher absorption in both the UV−visible and near-infrared regions as compared to thin film amorphous silicon making them a promising material for large area photovoltaics.

Acknowledgment. The authors thank A. Fadavi and M.H. Izadi for helpful discussions, R. Barber for technical support with PECVD equipment, and M. Collins for support with transmission and reflectance measurements. The work of M.M.A. and K.S.K. was supported by NSERC (Natural Science and Engineering Council of Canada), CFI (Canada Foundation for Innovation), and ORF (Ontario Research Fund). The work of M.P.A. was supported by the National Science Foundation under Grant No. 1001174.

REFERENCES AND NOTES

(1) Hu, L.; Chen, G. *Nano Lett.* **2007**, *7* (11), 3249–3252.
(2) Tsakalakos, L.; Balch, J.; Fronheiser, J.; Shih, M. Y.; LeBoeuf, S. F.; Pietrzykowski, M.; Codella, P. J.; Korevaar, B. A.; Sulima, O.; Rand, J.; Kumar, A. D.; Rapol, U. *J. Nanophotonics* **2007**, *01*, No. 013552.
(3) Hochbaum, Al.; Chen, R.; Delgado, R. D.; Liang, W.; Garnett, E. C.; Najarian, M.; Majumdar, A.; Yang, P. *Nature* **2008**, *451* (7175), 163–8.
(4) Cui, Y.; Zhong, Z. Z.; Wang, D.; Wang, W. U.; Lieber, C. M. *Nano Lett.* **2003**, *3* (2)), 149–152.
(5) Lauhon, L. J.; Gudiksen, M. S.; Wang, D.; Lieber, C. M. *Nature* **2002**, *420*, 57.
(6) Cui, L. F.; Ruffo, R.; Chan, C. K.; Peng, H.; Cui, Y. *Nano Lett.* **2008**, *9* (1), 491–495.
(7) Dong, Y.; Yu, G.; McAlpine, M. C.; Lu, W.; Lieber, C. M. *Nano Lett.* **2008,** *8* (2), 386–391.
(8) Stelzner, T.; Pietsch, M.; Andra, G.; Falk, F.; Ose, E.; Christiansen, S. *Nanotechnology* **2008**, *19*, 295203.
(9) Kelzenberg, M. D.; et al. *Nat. Mater.* **2010**, *9*, 239–244.
(10) Ma, D. D. D.; Lee, C. S.; Au, F. C. K.; Tong, S. Y.; Lee, S. T. *Science* **2003**, *299* (5614), 1874–1877.
(11) Shiri, D.; Kong, Y.; Buin, A.; Anantram, M. *Appl. Phys. Lett.* **2008**, *93*, No. 073114.
(12) Zhu, J.; Yu, Z.; Burkhard, G. F.; Hsu, C.; Connor, S. T.; Xu, Y.; Wang, Q.; McGehee, M.; Fan, S.; Cui, Y. *Nano Lett.* **2009**, *9*, 279.
(13) Taguchi, M.; et al. *Prog. Photovoltaics* **2000**, *8*, 503–513.
(14) Street, R. A. *Hydrogenated Amorphous Silicon*; Cambridge University Press: Cambridge, 1991; Section 1.2.4.
(15) Yu, D. P.; et al. *Appl. Phys. Lett.* **1998**, *72* (26), 3458–60.
(16) Holmes, J. D.; Johnston, K. P.; Doty, R. C.; Korgel, B. A. *Science* **2000**, *287*, 1471–3.
(17) Peng, K. Q.; Yan, Y. J.; Gao, S. P.; Zhu, J. *Adv. Mater.* **2002**, *14*, 1164.
(18) Wagner, R. S.; Ellis, W. C. *Appl. Phys. Lett.* **1964**, *4* (5)), 89.
(19) Givargizov, E. I. *J. Cryst. Growth* **1975**, *31*, 20–30.
(20) Westwater, J.; Gosain, D. P.; Tomiya, S.; Usui, S.; Ruda, H. *J. Vac. Sci. Technol., B* **1997**, *15* (3)), 554–557.
(21) Hofmann, S.; Ducati, C.; Neill, R. J.; Piscanec, S.; Ferrari, A. C.; Geng, J.; Dunin-Borkowski, R. E.; Robertson, J. *J. Appl. Phys.* **2003**, *94*, 6005.
(22) Wang, Y.; Schmidt, V.; Senz, S.; Gösele, U. *Nat. Nanotechnol.* **2006**, *1*, 186–189.
(23) Sunkara, M. K.; Sharma, S.; Miranda, R. *Appl. Phys. Lett.* **2001**, *79*, 1546.
(24) Iacopi, F.; Vereecken, P. M.; Schaekers, M.; Caymax, M.; Moelans, N.; Blanpain, B.; Richard, O.; Detavernier, C.; Griffiths, H. *Nanotechology* **2007**, *18*, 505307.
(25) Yu, J. Y.; Chung, S. W.; Heath, J. R. *J. Phys. Chem. B* **2000**, *104* (50), 11864–11870.
(26) Carter, J. D.; Qu, Y.; Porter, R.; Hoang, L.; Masiel, D. J.; Guo, T. *Chem. Commun.* **2005**, 2274.
(27) Kamins, T. I.; Williams, R. S.; Basile, D. P.; Hesjedal, T.; Harris, J. S. *J. Appl. Phys.* **2001**, *89* (2)), 1008–1016.
(28) Chen, Z. H.; Jie, J. S.; Luo, L. B.; Wang, H.; Lee, C. S.; Lee, S. T. *Nanotechnology* **2007**, *18*, 345502.
(29) Parlevliet, D.; Cornish, J. C. L. *Mater. Res. Soc. Symp. Proc.* **2007**, *989*, No. 0989-A23−03.
(30) Jeon, M.; Uchiyama, H.; Kamisako, K. *Mater. Lett.* **2009**, *63* (2), 246–248.
(31) Rohatgi, A.; Davis, J. R.; Hopkins, R. H.; McMullin, P. G. *Solid State Electron.* **1983**, *26* (11), pp. 1039–1051.
(32) Trumbore, F. A.; Isenberg, C. R.; Probansky, E. M. *J. Phys. Chem. Solids* **1958**, *9*, 60–69.
(33) Wu, C.; Crouch, C. H.; Zhao, L.; Carey, J. E.; Younkin, R. *Appl. Phys. Lett.* **2001**, *78*, 1850.
(34) Younkin, R.; Carey, J. E.; Mazur, E.; Levinson, J. A.; Friend, C. M. *J. Appl. Phys.* **2003**, *93*, 2626.

© 2010 American Chemical Society

DOI: 10.1021/nl102183x | *Nano Lett.* **2010,** *10,* 4093-–4098